Progress in Physics of Applied Materials 6 (2026), Serial Number 12, 257-263

Semnan University

Progress in Physics of Applied Materials

journal homepage: https://ppam.semnan.ac.ir/

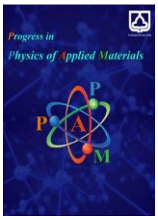

Synthesis and Investigation of Structural and Magnetic Properties of Double Perovskite $PrBaMn_2O_6$

Elham Jahedmadieh, Mohammad Hossein Ehsani*

Faculty of Physics, Semnan University, Semnan35195-363, Iran

A R T I C L E I N F O

Article history:
Received: 2 October 2025
Revised: 3 February 2026
Accepted: 3 February 2026
Published online: 11 April 2026

Keywords:
Double Perovskite;
Combustion Method;
Structural Properties;
Magnetic Properties.

A B S T R A C T

This study presents the synthesis and characterization of the double perovskite compound $PrBaMn_2O_6$ was synthesized using a combustion method. Thermogravimetric analysis (TGA) was employed to determine the optimal synthesis temperatures, while sintering was carried out under air to achieve phase purity. The structural and magnetic properties of the material were investigated using X-ray diffraction (XRD), Fourier transform infrared (FTIR) spectroscopy, field emission scanning electron imaging microscopy (FESEM), vibrating Sample Magnetometry (VSM) and Alternating Current Magnetic Susceptibility (AC susceptibility) analyses. Rietveld refinement using foolproof confirmed a dominant tetragonal structure with space group P4/mmm, accompanied by a minor hexagonal $BaMnO_3$-type phase. This dual-phase composition introduces lattice strain and partial disorder, which significantly influence the magnetic response. Magnetic measurements at room temperature indicated paramagnetic behavior, suggesting the absence of long-range magnetic ordering. The observed magnetization is attributed to the paramagnetic response of the material, as confirmed by both VSM and AC susceptibility measurements, with the latter revealing a suppressed transition below 200 K due to competing interactions from the secondary phase.

1. Introduction

With the rapid expansion of industrial activity and the continuous growth of the global population, energy demand has risen significantly. Despite progress in renewable energy technologies, much of today's energy production still depends on combustion of carbon-based fuels. This reliance, with air serving as the primary oxidizing agent, results in the emission of harmful gases such as CO_2, NO_x, and SO_x, which are major contributors to environmental pollution [1]. In response, researchers have been working to develop cleaner energy sources and advanced energy storage systems to reduce our dependence on fossil fuels. However, the transition to sustainable alternatives remains challenging due to technological and economic limitations.

Therefore, advancing new materials with enhanced catalytic and electronic properties is essential for optimizing energy efficiency and pollutant purification to prevent further environmental degradation. Among the materials gaining attention are perovskite compounds, known for their wide range of physical, magnetic, and electrical behaviors. In particular, double perovskites (DPs), with the general formula $AA'BB'O_6$, have shown great potential for energy-related applications [2]. These structures incorporate rare-earth or alkaline-earth ions at the A/A′ sites and transition metals from the 3d, 4d, or 5d series at the B/B′ sites. The precise arrangement of these cations is critical in determining the structural stability, electronic properties, and functional behavior of these materials [3]. Partial cation substitution is widely employed to tune the properties of perovskites by replacing specific

---

* Corresponding author.
E-mail address: ehsani@semnan.ac.ir

Cite this article as:

Jahedmadieh, E. and Ehsani, M.H., 2026. Synthesis and Investigation of Structural and Magnetic Properties of Double Perovskite $PrBaMn_2O_6$. *Progress in Physics of Applied Materials*, *6*(3), pp.257-263. DOI: **10.22075/ppam.2026.39247.1174**
© 2026 The Author(s). Progress in Physics of Applied Materials published by Semnan University Press. This is an open access article under the CC-BY 4.0 license. (https://creativecommons.org/licenses/by/4.0/)

ions at either the A-site or B-site within the lattice. For $CaMnO_3$, this involves substituting Sr^{2+} for Ca^{2+} at the A-site and Co^{3+} for Mn^{4+} at the B-site. Such substitutions can significantly modify the crystal symmetry, carrier concentration, and thermoelectric performance of the material, as evidenced by XRD, Raman spectroscopy, and electrical measurements [4]. The influence of B/B' cations on electronic properties is largely determined by their oxidation states, electron occupancy, and spin interactions, which can modify bonding environments and charge transport pathways [5]. The structural stability of $AA'BB'O_6$ compounds is strongly correlated to the arrangement of B/B' cations within their octahedral sites, the cation size, and the electronic structure associated with transition metals in the 3d and 4d orbitals [3]. Their diverse properties often stem from octahedral distortions and angular adjustments, which modify the crystal symmetry and influence electronic behavior. The $B'O_6$ octahedra establish a corner-sharing network, with A-site cations occupying the interstitial voids. To accommodate deviations from ideal ionic size ratios, these octahedra can expand, contract, or reorient, thus maintaining structural equilibrium [3,5].

Moreover, under electronic instabilities, the framework may undergo additional distortions, and cations can shift away from their equilibrium positions, altering local bonding environments. Such structural modifications, including cation displacements and charge disproportionation, are known to exert a significant impact on thermoelectric efficiency, spin polarization, and electrochemical activity [6]. In 2011, Aliev et al. investigated the double perovskite $PrBaMn_2O_6$ and reported two magnetic phases: a ferromagnetic phase with a Curie temperature (T_C) around 310–320 K and an A-type antiferromagnetic phase with a Néel temperature (T_N) between 200–270 K. The variation in these critical temperatures was attributed to differences in oxygen stoichiometry and synthesis conditions, highlighting the sensitivity of the compound's magnetic properties to sample preparation. In addition, the authors used direct calorimetric measurements to evaluate magnetocaloric behavior. Under low magnetic fields, they observed an inverse magnetocaloric effect with an adiabatic temperature change of approximately $\Delta T_{ad} \approx 0.13$ K [7].

Recent investigations have shown that A-site ordering in $PrBaMn_2O_6$ plays a pivotal role in determining both its structural and magnetic characteristics. The layer-by-layer arrangement of Pr^{3+} and Ba^{2+} ions lead to a tetragonal crystal symmetry and stabilizes distinct magnetic phases compared to disordered analogs. Samples with high A-site ordering exhibit a ferromagnetic metallic state near room temperature, whereas partial disordering induced by thermal annealing leads to the coexistence of multiple magnetic phases and a reduction in T_C. Moreover, the degree of ordering directly influences the magneto-transmission effect, as changes in cation arrangement alter the concentration and mobility of delocalized charge carriers near the magnetic transition point [8]. Among the most significant properties of this class of materials is their supercapacitive behavior. Perovskite oxides, owing to their high oxygen vacancy concentration, rapid oxygen ion diffusion, and substantial charge-hopping density, represent highly promising electrode candidates for interlayer-type oxygen-ion supercapacitors. In such systems, capacitance arises from an anion-intercalation mechanism, in which surface and interlayer redox reactions involving oxygen ions within the crystal lattice contribute to charge storage. Therefore, a high concentration of oxygen vacancies is essential, as these vacancies serve as the principal charge carriers. Notably, this mechanism enables high energy storage capacity without requiring an extensive specific surface area. Consequently, such layered structured materials can function effectively as oxygen anion-type electrode components in supercapacitor applications [9].

In general, the oxides $LnBaMn_2O_{5+\delta}$ (Ln = Ce, Pr, Gd, Y) exhibit distinct redox transitions between two separate phases at $\delta = 0$ and 0.5, while a broader compositional range is stabilized in the third phase at $\delta = 1$ [10]. Achieving a pure phase in this class of materials remains a significant challenge during synthesis. As demonstrated in doped perovskite systems such as $LaMn_{1-x}Cu_xO_3$, synthesis conditions, particularly the calcination temperature and doping strategy play a crucial role in determining the structural, magnetic, and transport properties of the final material [11]. As previously noted, the synthesis method plays a crucial role in determining the final properties of the material; therefore, selecting an efficient, cost-effective approach that minimizes processing time is essential. From the simplest oxide systems to the most complex perovskite structures, the choice of synthesis route critically influences phase purity, microstructure, and ultimately the material's functional properties [12]. Once an optimal synthesis route is chosen such as solid-state reaction, sol-gel, combustion synthesis, or co-precipitation, the temperature becomes a critical factor due to its role in phase formation. The calcination temperature, commonly applied in sol-gel, co-precipitation and combustion methods to remove organics and decompose precursors. the sintering temperature, typically used in solid-state and sol-gel methods to achieve complete crystalline phase formation and densification. the post annealing conditions, usually performed as a final step under controlled gas atmospheres such as O_2, H_2, or Ar to improve structural stability and adjust oxygen stoichiometry, must all be carefully optimized to ensure phase purity. Since the physical, electronic, and catalytic properties of double perovskites are highly sensitive to synthesis conditions, this study focuses on establishing an effective route for synthesizing of $PrBaMn_2O_6$ nanoparticles while investigating the impact of temperature control and processing parameters on phase purity and functional characteristics [13]. Under electronic instability conditions, structural modifications, such as cation displacements and charge disproportionation, can strongly influence local bonding environments, thereby affecting thermoelectric efficiency, spin polarization and electrochemical activity [6].

Given the high sensitivity of double perovskites to synthesis conditions, limited attention has been devoted to the systematic optimization of $PrBaMn_2O_6$ synthesis, particularly in relation to phase purity and thermal processing. This study aims to address this gap by establishing a controlled synthesis route and correlating synthesis parameters with structural and functional outcomes, ultimately contributing to the development of high-performance perovskite materials for energy and environmental applications.

2. Experimental

The polycrystalline $PrBaMn_2O_6$ perovskite was synthesized by the combustion method. The raw materials $Ba(NO_3)_2$, $Pr(NO_3)_3{\cdot}6H_2O$, $Mn(NO_3)_3{\cdot}4H_2O$, in a molar ratio of 1:1:2 and $C_{12}H_{22}O_{11}$ were measured in stoichiometric quantities and then the mixture was dissolved in 20cc deionized water. A homogeneous solution was obtained by ultrasonic treatment at 70 °C for 30 minutes and was then subjected to direct thermal treatment by transferring it into a furnace pre-set to 500 °C under air to facilitate the combustion process. After cooling, the reaction product was ground using a mortar and pestle. The resulting powder was sintered at 1300 °C in air to obtain the final sample. Based on the XRD results, additional heat treatments were performed at 900 °C under 95% argon atmosphere and at 800 °C under hydrogen atmosphere in order to obtain a single-phase and homogeneous product. Furthermore, sintering at different temperatures under air was also tested. However, XRD analysis revealed that the sample sintered at 1300 °C in air exhibited the most stable structural phase, Therefore, only this optimized sample is reported and discussed in the manuscript. Microstructure and morphology of the sample were studied by XRD (ADVANCE-D8 model) using a Cu-Kα radiation source and by field emission scanning electron microscopy (FESEM). The XRD data were analyzed by Rietveld refinement using the foolproof software. Infrared transmission spectra were measured using a SHIMADZU FT-IR spectrophotometer, model 8400s, in KBr pellets. The magnetic hysteresis loop was measured at room temperature using a Vibrating Sample Magnetometer (VSM, Lakeshore model). AC magnetic susceptibility was measured using a Lake Shore AC Susceptometer.

3. Results and Discussion

The TGA results presented in Figure 1 show a minor weight loss of approximately 3.29% occurring between 93°C and 462°C. This weight reduction is likely attributed to the evaporation of absorbed moisture, the release of structural water, or the volatilization of organic compounds such as sucrose or residual nitrates. Notably, nitrate decomposition generally does not initiate within this temperature range. However, between 462°C and 574°C, a substantial weight loss of 12.11% suggests the onset of significant thermal reactions. In this interval, the decomposition of metal nitrates including barium nitrate, manganese nitrate and praseodymium nitrate, takes place.

Concurrently, sucrose undergoes complete thermal degradation, releasing sufficient energy to drive the decomposition processes. Therefore, the temperature of 500°C is identified as the combustion phase. In the final stage, from 570°C to 800°C, an additional weight loss of approximately 7.89% corresponds to the completion of nitrate decomposition and the oxidation of residual organic matter. This stage leads to the formation of stable metal oxides, such as manganese oxide, barium oxide, and related compounds, indicating the materials transition to a thermodynamically stable state. For the complete formation of the perovskite phase, elimination of residual impurities, and achievement of a stable crystalline structure, temperatures higher than 800 °C are required.

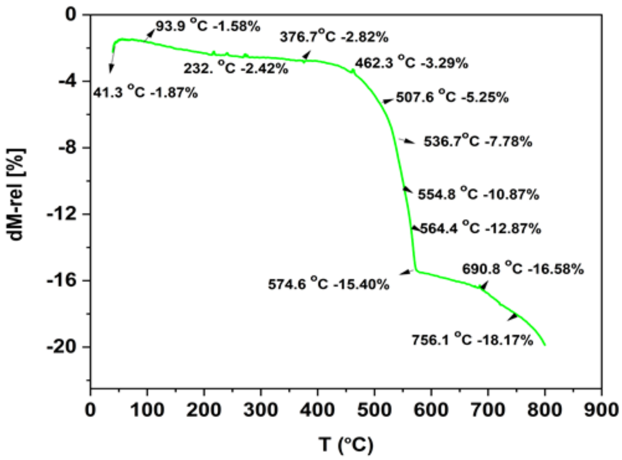

Fig. 1. TGA of the sample performed under air atmosphere.

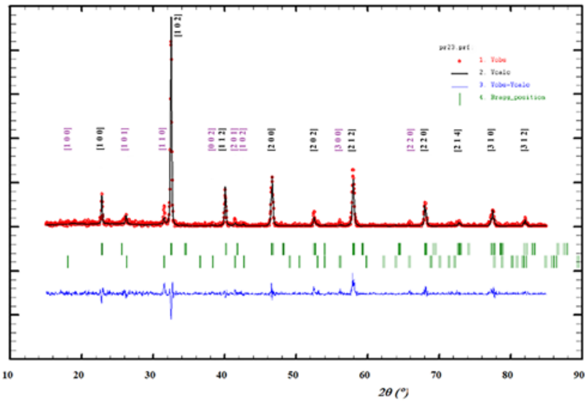

Fig. 2. XRD pattern measured at RT with Rietveld refinement.

The room-temperature X-ray diffraction (XRD) pattern presented in Figure 2 exhibits a primary set of diffraction peaks consistent with an A-site layered double perovskite crystal structure. However, additional reflections were also detected, indicating the presence of a secondary phase. Rietveld refinement of the XRD data confirmed that the primary phase crystallizes in the tetragonal P4/mmm space group (92.73%), while 7.27% corresponds to a secondary hexagonal $P6_3mc$ phase related to $BaMnO_3$. The quality of the Rietveld refinement (χ^2 = 1.8). Rajabi et al. observed orthorhombic–rhombohedral phase coexistence at intermediate composition, which modifies lattice parameters and diffraction intensities and therefore complicates structural assignment [14]. The Williamson–Hall calculation indicated an average crystallite size of ~549 Å with a lattice strain of ~$1.56{\times}10^{-4}$, whereas the second phase exhibited a smaller crystallite size of ~433 Å with a lattice strain of ~$1.67{\times}10^{-4}$. Initial Crystallographic data were obtained from the Materials Project database ($PrBaMn_2O_6$: mp-19274; $BaMnO_3$: mp-1205336, accessed December 12, 2025) [15]. Detailed results from the Rietveld refinement are summarized in Table 1. Parameter c for the tetragonally sample is doubled as a consequence of A-site ordering between L^{3+} and Ba^{2+} ions. Direct evidence of A-site ordering from XRD is the [001] superlattice reflection, typically observed around 2θ≈17° ; this reflection attests to an A-site modulation along the c axis of the tetragonal unit cell, with layers preferentially occupied by either Ba or L cations. It is important to note that the intensity of the [001] reflection depends critically on the scattering contrast between L^{3+} and Ba^{2+}. If long-range A-site ordering is absent or substantially weakened, the [001] superlattice peak will be strongly suppressed and may become effectively unobservable. Under such circumstances, even a minor amount of a hexagonal secondary phase (≈7.27%) can produce a pronounced fundamental [100] reflection that falls in the same angular region. Because the hexagonal and tetragonal lattices possess different lattice parameters, the [100] reflection of $BaMnO_3$ appears at a distinct 2θ position and candominate the diffraction pattern in the region where the suppressed [001] reflection would otherwise be expected. Consequently, the weakness or absence of the [001] peak in our data is consistent with A-site disorder and the presence of a small hexagonal $BaMnO_3$ secondary phase, which together explain the observed diffraction features [16].

Table 1. Rietveld refined structural parameters.

lattice parameters	Tetragonal	Hexagonal
Space group	P4/mmm (92.73 %)	$P6_3mc$ (7.27 %)
a (Å)	3.891	5.676
b (Å)	3.891	5.676
c (Å)	7.80	4.70
V $(Å)^3$	118.16	131.115
α (deg)	90	90
β (deg)	90	90
γ (deg)	90	120

$BaMnO_3$ crystallizes predominantly in a twisted hexagonal system characterized by dense stacking of BaO_3 layers. Structural defects within this lattice lead to notable variations in both structure and physical properties, including magnetism and insulating behavior. Hexagonal arrangements often exhibit reduced symmetry due to different oxygen octahedra stacking modes [17]. In the $BaMnO_3$-type hexagonal phase (space group $P6_3mc$), Mn^{4+} ions occupy C_3v sites within face-sharing MnO_6 trigonal antiprisms aligned along the c-axis. Unlike conventional double perovskites with corner-sharing geometries, this topology gives rise to distinct properties, notably a spin-glass state arising from the competition between ferromagnetic and antiferromagnetic interactions [18]. Similar phenomena have been observed in La_2MnNiO_6 compounds, where local strain and octahedral tilting induced phase instability and domain formation [19]. Moreover, a previous study on BaMn-based phases has shown that external pressure can induce structural transformations and symmetry breaking, as exemplified in the DP Ba_2SmBiO_6 system [20].

FESEM images of the compound are shown in Figure 3. The coexistence of two different phases, tetragonal and hexagonal, significantly influences the particle morphology, primarily by introducing heterogeneous, anisotropic growth behaviors and interfacial strain effects.

This phenomenon results in a broad distribution of particle sizes and shapes, reflecting the interplay between crystal lattice, thermodynamics, and kinetics during synthesis. The tetragonal phase as the main and more stable phase, promotes to formation uniform crystals, resulting in large polygonal particles. In contrast, the secondary phase is less stable and has a different lattice anisotropy, supporting irregular morphologies with small particles.

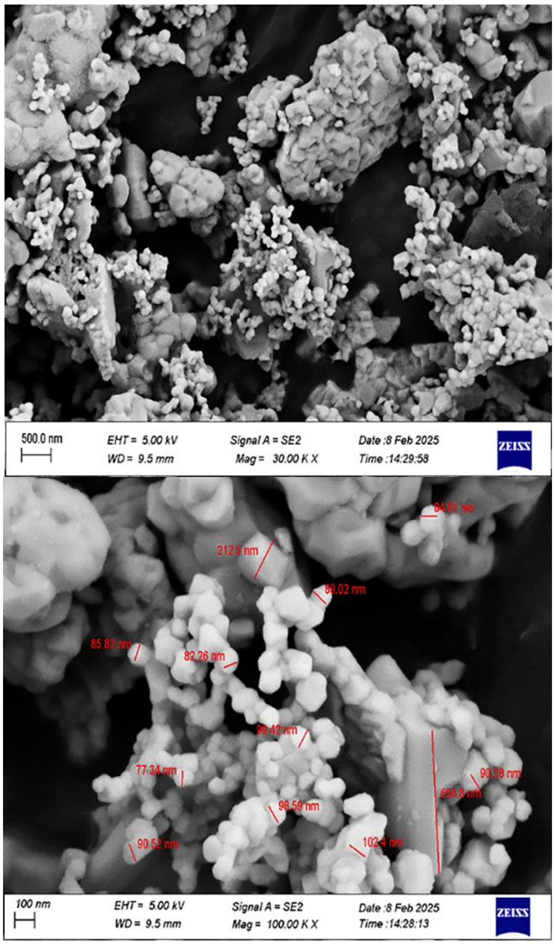

Fig. 3. The FESEM images of the sample in different scales.

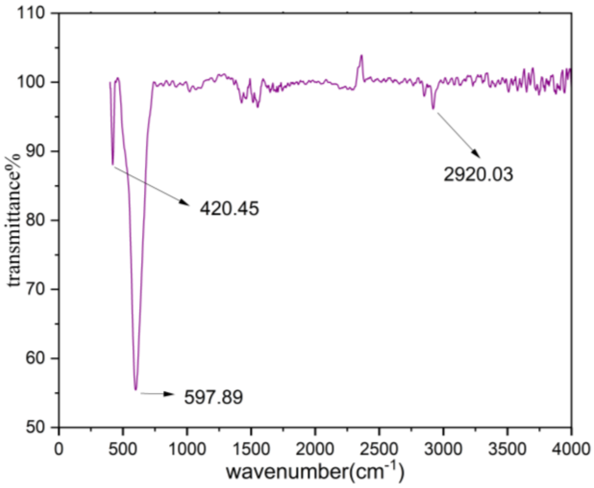

Fig. 4. Room temperature FT-IR transmission for the sample.

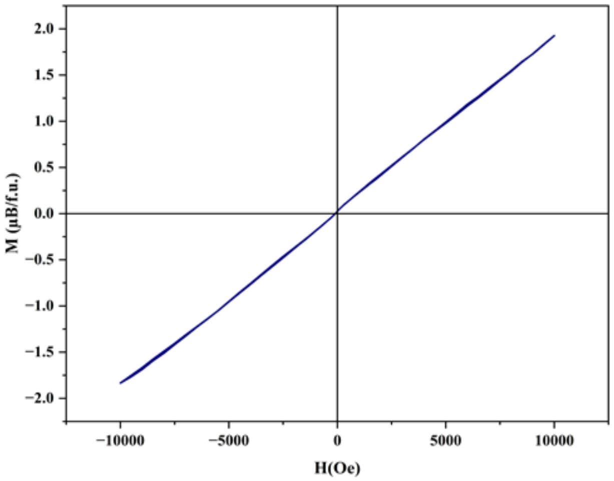

Fig. 5. Field dependence of magnetization for the sample at room temperature.

The IR spectra shown in Figure 4 exhibit an absorption band at 2920 cm^{-1}, which is likely due to C–H stretching vibrations resulting from the adsorption of atmospheric organic compounds on the sample surface [21]. In addition, bands observed at 420 cm^{-1} and 597 cm^{-1} correspond to Mn–O stretching vibrations within MnO_6 octahedra a typical feature of the manganite structure [22].

The hysteresis curve measured at room temperature is presented in Figure 5 revealing that the synthesized sample exhibits purely paramagnetic behavior. No remanence or coercivity is observed, confirming the absence of magnetic ordering. This finding aligns with the structural properties of the material, which consists primarily of a tetragonal phase with a minor hexagonal phase. The dominance of the tetragonal phase suggests that spontaneous magnetization does not occur, while the presence of the hexagonal phase may introduce weak competing interactions, thereby further suppressing magnetic ordering. Additionally, potential lattice strain or cation disorder within the A-site framework could influence the magnetic response, further reinforcing the sample's paramagnetic nature.

$PrBaMn_2O_6$ exhibits a magnetic transition near 280–300 K. A-site ordered structures show higher Curie temperatures (~320 K), whereas a disordered one displays much lower values (~140 K). The degree of A-site cation ordering strongly influences the crystal structure, magnetic behavior, and electrical transport. In tetragonal structures with alternating L^{3+}/Ba^{2+} layers along the c-axis, the transition temperature to the paramagneticstate increases significantly [23]. These pronounced variations can be interpreted using the Goodenough-Kanamori rules for 180° super-exchange interactions, taking ionic size effects into account. A spin-glass state emerges when substantial fluctuations occur in the Mn-O-Mn bond angle, which results from the mismatch between the ionic radii of L and D cations. An increase in the average A-site ionic radius $\langle r_A \rangle$ brings the Mn-O-Mn angle closer to 180°, thereby strengthening exchange interactions, whereas orbital disorder may reverse the sign of these interactions as the angle decreases [24]. Random distribution of L and D ions produces local dispersion in bond angles, which under critical conditions allows ferromagnetic features to appear.

In manganites, orbital and charge states govern magnetic ordering: charge-ordered compounds behave as antiferromagnetic insulators, while charge-disordered ones exhibit ferromagnetic metallic behavior [16]. Furthermore, an external magnetic field can induce a transition from the antiferromagnetic to the ferromagnetic state, accompanied by drastic changes in resistivity. Such behavior resembles spin-glass phenomena and arises from the competition between randomly distributed ferromagnetic and antiferromagnetic interactions [23].

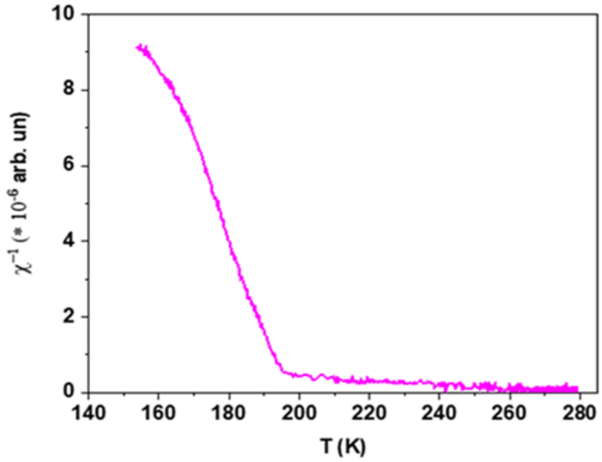

Fig. 6. The real part of susceptibility of the sample.

The real part of the AC susceptibility measured at a frequency of 111 Hz is presented in Figure 6. A sharp decrease in susceptibility below 200 K, followed by a linear trend above this temperature, suggests a significant transition and indicates a paramagnetic response, consistent with the VSM measurement. For instance, disordered $EuBaMn_2O_6$ exhibits spin-glass behavior with a freezing temperature of $T_f \approx 40$ K, whereas the ordered phase is an inhomogeneous ferromagnet with $T_C \approx 260$ K. In compounds with Pr and Nd, the magnetic ordering temperature decreases to ~160 K and ~80 K, respectively.

Proximity to the ferromagnetic–antiferromagnetic boundary ($x \approx 0.5$ in $L_{1-x}Ba_xMnO_3$) can also generate antiferromagnetic domains. A-site ordering promotes translational symmetry in Mn–O–Mn bond angles and reduces Mn–O bond lengths, thereby favoring ferromagnetism and enhancing the magnetic ordering temperature, while A-site randomness suppresses both ferromagnetic and A-type antiferromagnetic transitions, leading to a magnetic glassy state. Experimental and theoretical studies confirm that phenomena such as colossal magnetoresistance (CMR) and electronic phase separation arise from the critical competition between ferromagnetic metallic states and antiferromagnetic charge–orbital ordered states, which are highly sensitive to A-site disorder [16]. In $RBaMn_2O_6$ compounds, novel properties originate not only from the absence of A-site randomness but also from the layered $BaO–MnO_2–RO–MnO_2$ stacking sequence along the c-axis. In strongly disordered systems such as $Pr_{0.5}Ba_{0.5}MnO_3$, magnetic glassy behavior results from disorder effects that hinder long-range magnetic order through the competition of randomly distributed ferromagnetic and antiferromagnetic interactions [25]. In the present sample, Rietveld refinement confirms the coexistence of a tetragonal main phase and a minor hexagonal phase, which introduces lattice strain and disrupts cationic arrangement. This partial disorder suppresses long-range magnetic ordering and shifts transition temperatures, as evidenced by AC susceptibility and VSM results. These effects are consistent with previous studies on $RBaMn_2O_6$ systems, where A-site disorder and multiphase coexistence modify spin, charge, and orbital interactions [26].

4. Conclusions

In this study, the double perovskite $PrBaMn_2O_6$ was successfully synthesized using the combustion method. Structural analyses revealed that the primary phase crystallizes in the tetragonal P4/mmm space group, while a secondary $BaMnO_3$ phase adopts the hexagonal $P6_3mc$ symmetry. FESEM micrographs confirmed the coexistence of these two phases, resulting in large polygonal grains alongside irregular smaller particles. IR spectra exhibited characteristic Mn–O stretching vibrations in MnO_6 octahedra. Magnetic measurements demonstrated that the sample exhibits purely paramagnetic behavior at room temperature, with no remanence or coercivity, indicating the absence of long-range magnetic ordering. AC susceptibility revealed a pronounced transition below 200 K, attributed to the minor hexagonal phase, which introduces competing interactions and modifies the expected transition temperature. Overall, these findings highlight that A-site cation ordering/disordering, lattice strain, and phase coexistence play decisive roles in tuning the magnetic response. Therefore, interpreting the magnetic behavior of Ba-containing double perovskites requires consideration of oxygen stoichiometry, cation distribution, and phase purity beyond classical tolerance factor models. These results not only clarify the structural–magnetic correlations in $PrBaMn_2O_6$ but also highlight the broader potential of Ba-containing double perovskites as tunable platforms for spintronic applications, magnetic sensors, and energy-related devices. The demonstrated sensitivity to A-site ordering, lattice strain, and oxygen stoichiometry suggests that these materials can be engineered beyond classical tolerance factor models, opening pathways for designing multifunctional oxides with tailored properties.

Funding Statement

This research received no specific grant from any funding agency.

Conflicts of Interest

Professor Mohammad Hossein Ehsani, the corresponding author of this paper is the current Director-in-Charge of Progress in Physics of Applied Materials (PPAM), but he has no involvement in the peer review process used to assess this work submitted to the Journal. This paper was assessed, and the corresponding peer review managed by Dr. Sanaz Alamdari, the Executive Manager of PPAM.

Authors Contribution Statement

All authors contributed equally to this work.

References

[1] Kudyakova, V.S., Politov, B.V., Chukin, A.V., Markov, A.A., Suntsov, A.Y. and Kozhevnikov, V.L., 2020. Phase stability and oxygen storage capacity of $PrBaMn_2O_6$. *Materials Letters, 269*, p.127650.

[2] Mayer, K., Piesenberger, S., Penthor, S., Proll, T. and Hofbauer, H., 2018. Chemical looping combustion using two different perovskite based oxygen carriers: a pilot study. *Energy Technol (Weinh), 6*, pp.2333-2343.

[3] Basavarajappa, M.G. and Chakraborty, S., 2022. Rationalization of double perovskite oxides as energy materials: a theoretical insight from electronic and optical properties. *ACS Materials Au, 2*, pp.655-664.

[4] Mary, S.B., Mohan, K. and Krishnan, M.M., 2024. Effect of A-site and B-site ion substitution on the electrical and thermoelectric properties of nanostructured perovskite $CaMnO_3$. *Journal of Materials Science: Materials in Electronics, 35*, p.600.

[5] Krichene, A., Solanki, P.S., Rayaprol, S., Ganesan, V., Boujelben, W. and Kuberkar, D.G., 2015. B-site bismuth doping effect on structural, magnetic and magneto transport properties of $La_{0.5}Ca_{0.5}Mn_{1-x}Bi_xO_3$. *Ceramics International, 41*, pp.2637-2647.

[6] Kishna Murthy, J., Devi Chandrasekhar, K., Mahana, S., Topwal, D. and Venimadhav, A., 2015. Giant magnetocaloric effect in Gd_2NiMnO_6 and Gd_2CoMnO_6 ferromagnetic insulators. *Journal of Physics D: Applied Physics, 48*, p.355001.

[7] Aliev, A.M., Gamzatov, A.G., Batdalov, A.B., Kalitka, V.S. and Kaul, A.R., 2011. Specific heat and low-field magnetocaloric effect in A-site ordered $PrBaMn_2O_6$ manganite. *Philosophical Magazine Letters, 91*, pp.354-360.

[8] Mostovshchikova, E.V., Sterkhov, E.V., Naumov, S.V., Ermolov, N.S., Uporov, S.A. and Titova, S.G. 2021. Effect of A-site ordering on IR absorption and magneto transmission in $PrBaMn_2O_6$ double manganite. *Journal of Magnetism and Magnetic Materials, 538*, pp.168247.

[9] Liu, Y., Wang, Z., Veder, J.P.M., Xu, Z., Zhong, Y., Zhou, W., Tade, M.O., Wang, S., and Shao, Z. 2018. Highly defective layered double perovskite oxide for efficient energy storage via reversible pseudocapacitive oxygen-anion intercalation. *Advanced Energy Materials, 8*, p.1702604.

[10] Tonus, F., Bahout, M., Dorcet, V., Gauthier, G. H., Paofai, S., Smith, R.I. and Skinner, S.J., 2016. Redox behavior of the SOFC electrode candidate $NdBaMn_2O_{5+\delta}$ investigated by high-temperature in situ neutron diffraction: first characterisation in real time of an $LnBaMn_2O_{5.5}$ intermediate phase. *Journal of Materials Chemistry A, 4*, pp.11635-11647.

[11] Kameli, P., Vaezi, H., Ehsani, M., Aslibeiki, B. and Salamati, H., 2021. Structual, magnetic, and transport properties of $LaMn_{1-x}Cu_xO_3$ (x= 0-0.125) ceramics. *Advanced Ceramics Progress, 7*, pp.1-10.

[12] Kafi, L. and Khademinia, Sh., 2022. Fabrication, characterization, and photocatalytic degradation of malachite green by CuO nanocatalyst. *Progress in Physics of Applied Materials, 2*, pp.83–92.

[13] Shalamova, A.M., Samigullina, R.F., Chukin, A.V. and Suntsov, A. Y., 2023. Evolution of crystal structure and redox activity of $LnBaMn_2O_{6-\delta}$ upon various external conditions: in-situ

characterization. *Journal of Materials Science, 58*, pp.16634-16650.

[14] Rajabia, Y., Gholizadeha, A. and Gorzoddina, M., 2025. Investigating the Nonlinear Optical Behavior of $La_{1-x}Ca_xCo_{0.5}Mg_{0.5}O_3$ Perovskites. *Progress in Physics of Applied Materials, 5*, pp.47–52.

[15] Jain, A., Ong, S.P., Hautier, G., Chen, W., Richards, W.D., Dacek, S., Cholia, S., Gunter, D., Skinner, D., Ceder, G. and Persson, K.A., 2013. The materials Project: A materials genome approach to accelerating materials innovation. *APL Materials, 1(1),* p.011002.

[16] Trukhanov, S.V., Troyanchuk, I.O., Hervieu, M., Szymczak, H. and Barner, K., 2002. Magnetic and electrical properties of $LBaMn_2O_{6-\delta}$ (L=Pr, Nd, Sm, Eu, Gd, Tb) manganites. *Physical Review B, 66*, p.184424.

[17] Wang, H., Li, X., Chen, Z. and others, 2025. Magnetism, magnetoresistance, and temperature coefficient of resistance of the $BaMnO_3$ compound. *Applied Physics, 137*, p.045301.

[18] Stanislavchuk, T.N., Litvinchuk, A.P., Hu, R., Jeon, Y.H., Ji, S.D., Cheong, S.W. and Sirenko, A.A., 2015. Optical properties, lattice dynamics, and structural phase transition in hexagonal 2H-$BaMnO_3$ single crystals. *Physical Review B, 92*, p.134308.

[19] Spurgeon, S.R., Sushiko, P.V., Devaraj, A., Du, Y., Droubay, T. and Chambers, S.A., 2018. Onset of phase separation in the double perovskite oxide La_2MnNiO_6. *Physical Review B, 97,* p.134110.

[20] Wang, Y., Zhang, L., MA, S., Zhao, Y., Tan, D. and Chen, B., 2021. Octahedral tilting dominated phase transition in compressed double perovskite Ba_2SmBiO_6. *Applied Physics Letters, 118*. p.231903.

[21] Volkov, D.S., Rogova, O.B. and Proskurnin, M.A., 2021. Organic matter and mineral composition of silicate soils: FTIR comparison study by photoacoustic, diffuse reflectance, and attenuated total reflection modalities. *Agronomy, 11(11),* p.2149.

[22] Ao, R., Ma, L., Guo, Z., Yang, J., Mu, L., Yang, J. and Wei, Y., 2020. No oxidation performance and kinetics analysis of $BaMO_3$ (M = Mn, Co) perovskite catalysts. *Environmental Science and Pollution Research, 28,* pp.6929-6940.

[23] Nakajima, T., Kageyama, H. and Ueda, Y., 2004. Dramatic change of magnetic property in the A-site ordered/disordered manganites $PrBaMn_2O_6/Pr_{0.5}Ba_{0.5}MnO_3$. *Magnetism and Magnetic Materials, 272-276*, p.405-406.

[24] Haji, R. and Khoshnoud, D., 2026. Structural, Magnetic, and Electrical Properties of $REFe_{0.7}Cr_{0.3}O_3$ (RE= La, Pr, Nd, Sm, and Gd) Compounds. *Progress in Physics of Applied Materials, 6*, pp.57–68.

[25] Mostovshchikova, E.V., Sterkhov, E.V., Pryanichnikov, S.V., Vedmid, L.B. and Titova, S.G., 2023. A-Site order-disorder evolution in double manganites $RBaMn_2O_6$ (R = Pr, Nd). *physics of metals and metallography, 124*, pp.1703-1715.

[26] Aliev, A.M., Gamzatov, A.G., Batdalov, A.B., Kalitka, V.S. and Kaul, A.R., 2011. Direct and inverse magnetocaloric effects in A-site ordered $PrBaMn_2O_6$ manganite. *Alloys and Compounds, 509*, pp.L165-L167.